AGU

PUBLICATIONS

Estimating phytoplankton primary productivity in the Changjiang estuary, East China Sea from coupled Fast Repetition Rate (FRR) fluorometry and Chlorophyll-a measurements

Yuanli Zhu[1,2], David J. Hughes[3], Yuanyuan Feng[4], Thomas J. Browning[5], Ping Du[1,2,7], Qicheng Meng[6,7], Shengqiang Wang[8], Bing Wang[1,2,7], Dewang Li[1,2,7], Zhibing Jiang[1,2,7], Jiangning Zeng[1,2,7]

[1]Key Laboratory of Marine Ecosystem Dynamics, Ministry of Natural Resources, Second Institute of Oceanography, Hangzhou, 310012, PR China
[2]Key Laboratory of Nearshore Engineering Environment and Ecological Security of Zhejiang Province, Hangzhou, 310012, PR China
[3]Australian Institute of Marine Science, Townsville, QLD, Australia
[4]School of Oceanography, Shanghai Jiao Tong University, Shanghai, PR China
[5]Marine Biogeochemistry Division, GEOMAR Helmholtz Centre for Ocean Research, Kiel, Germany
[6]State Key Laboratory of Satellite Ocean Environment Dynamics, Second Institute of Oceanography, Ministry of Natural Resources, Hangzhou, 310012, PR China
[7]Observation and Research Station of Marine Ecosystem in the Yangtze River Delta, Ministry of Natural Resources, Hangzhou, 310012, PR China
[8]School of Marine Sciences, Nanjing University of Information Science and Technology, Nanjing, 210044, Jiangsu, PR China

Corresponding author: Yuanli Zhu (ylzhu@sio.org.cn)

Key Points:

- Parallel *in-situ* measurements of net primary productivity and Fast Repetition Rate fluorometry were conducted in the Changjiang estuary.

- We observed substantial variations of phytoplankton photophysiology and net PP in this dynamic system.

- A generalized additive model was developed to predict net PP, providing a high-throughput approach for assessing regional PP.

Abstract

Phytoplankton primary productivity (PP) varies significantly over environmental gradients, particularly in physically-dynamic systems such as estuaries and coastal seas. As the Changjiang River runoff peaks during summer time, large environmental gradients appear in both the Changjiang estuary and adjacent East China Sea (ECS), likely driving significant variability in PP. As satellite models of PP often underperform in coastal waters, we aimed to develop a novel approach for net PP estimation in such a dynamic environment. Parallel *in situ* measurements of Fast Repetition Rate (FRR) fluorometry and carbon (C) uptake rates were conducted for the first time in this region during two summer cruises in 2019 and 2021. A series of ^{13}C-incubations (n=31) were performed, with measured PP ranging from ~6 - 1700 mgC m^{-3} d^{-1}. Net PP values were significantly correlated with salinity ($r = 0.45$), phytoplankton chlorophyll *a* (Chl-a, $r = 0.88$), Photosystem II (PSII) functional absorption cross-section (σ_{PSII}, $r = -0.76$) and maximum PSII quantum yield (F_v/F_m, $r = 0.59$). Stepwise regression analysis showed that Chl-a and σ_{PSII} were the strongest predictors of net PP. A generalized additive model (GAM) was also used to estimate net PP considering nonlinear effects of Chl-a and σ_{PSII}. We demonstrate that GAM outperforms linear modelling approaches in predicting net PP in this study, as evidenced by a lower root mean square error (~140 vs. 250 mgC m^{-3} d^{-1}). Our novel approach provides a high resolution means to examine carbon cycling dynamics in this important region.

Plain Language Summary

The East China Sea (ECS) has a complex current system that creates a highly dynamic physical environment for phytoplankton, particularly during the summer months. Net primary productivity (PP) is highly variable in this region, but characterising the spatial patterns in PP is difficult due to the lack of a high-resolution data collecting method. Therefore, there is a strong need for a quick and easily implemented method for monitoring PP to capture variations in this dynamic system. Based on parallel measurements of phytoplankton biomass and photophysiology, we have developed a model that allows us to rapidly and easily assess regional PP at a high resolution. The high data volume potentially provided by our net PP model could not only contribute to a better understanding of PP variations in such a dynamic environment, but also help fill the large gaps in field data needed for validating satellite-based primary productivity models.

1 Introduction

Phytoplankton primary productivity (PP) is a key process mediating the transfer of carbon (C) between the atmosphere and ocean interior, and thus plays a key role in regulating the global climate. However, PP varies greatly over space and time, depending upon environmental conditions including light, temperature and nutrient availability, together with the composition of

66   the phytoplankton community (Arrigo et al., 2000; Behrenfeld & Falkowski, 1997; Behrenfeld et

67   al., 2006; Cermeño et al., 2005; Marra, 2015; Moore et al., 2008; Ning et al., 1988; Platt & Jassby,

68   1976). Estimation of phytoplankton PP is therefore extremely challenging, particularly within

69   physically-dynamic systems such as estuaries and coastal waters (Gong and Liu, 2003; Firme et

70   al. 2023).

71   Satellite assessments of phytoplankton PP based on ocean color are routinely used in the

72   open ocean over large scales (Arrigo et al., 2008; Behrenfeld et al., 2005; Kameda & Ishizaka,

73   2005; Lee et al., 2015; Ning et al., 1998), yet are not easily applied to shallow coastal regions due

74   to interference from colored dissolved organic matter (CDOM), suspended sediment and land run-

75   off (Moreno-Madriñán & Fischer, 2013). Consequently, PP estimates for estuaries and coastal

76   regions are largely derived from direct, *in situ* observations (Cloern et al., 2014), usually performed

77   via carbon isotope (^{14}C or ^{13}C) incubations (Hama et al., 1983; Nielsen, 1952). While carbon

78   isotope methods are highly-sensitive, they also require long incubation periods, resulting in a very

79   low sampling resolution (Morelle et al., 2018). The lack of spatial and temporal coverage afforded

80   by incubation-based approaches limits our ability to fully understand environmental controls upon

81   PP variability in dynamic coastal waters (Cloern et al, 2014).

82   Fast Repetition Rate (FRR) fluorometry is a bio-optical technique capable of non-

83   invasively evaluating changes in photosystem II (PSII) photochemistry – allowing estimation of

84   phytoplankton productivity as photosynthetic electron transport rates (ETRs) (Kolber & Falkowski,

85   1993; Kolber et al., 1998). FRR fluorometry has rapidly become a widely-used oceanographic tool

86   for evaluating photosynthetic rates in coastal and open ocean waters (Cermeño et al., 2005; Hughes

87   et al., 2020; Moore et al., 2003; Robinson et al., 2014; Schuback et al., 2015; Suggett et al., 2006).

88   However, estimation of PP from FRR flurometery measurements requires conversion of ETRs to

89   C-uptake rates - i.e., from a photosynthetic "currency" of electrons to carbon (see Suggett et al.,

90   2009). This conversion requires knowledge (or assumption) of: i) the number of PSII reaction

91   centers per Chl-a (n_{PSII}), ii) the electron requirement for carbon fixation (K_C, or $\Phi_{e,C}$) and iii) an

92   appropriate spectral correction factor (scf) to account for spectral properties of the *in-situ* light

93   field versus the absorption spectra of the phytoplankton sample (reviewed by Hughes et al. 2018a).

94   All three parameters exhibit considerable variability but are not easily measured under field

95   conditions (Oxborough et al., 2012; Suggett et al., 2011), thus assumed values are often used,

96 which can introduce significant uncertainty into PP estimates (Cheah et al., 2011; Fujiki et al.,

97 2008; Kromkamp et al., 2008; Raateoja et al., 2004; Smyth et al., 2004; Zhu et al., 2016, 2019).

98 Importantly, ETRs are constructed from specific fluorescence parameters that are

99 retrievable from the single-turnover FRR measurement protocol (see Hughes et al. 2018a;

100 Schuback et al. 2021). These include the maximum quantum efficiency of PSII (F_v / F_m) and the

101 functional absorption cross-section of PSII (σ_{PSII}). Under actinic light, both F_v / F_m and σ_{PSII} are

102 modified according to how the absorbed light is utilized by PSII and as such, F_v / F_m and σ_{PSII} are

103 both likely (in)directly related to C-fixation, since light absorption is one of the key factors

104 governing PP (Behrenfeld et al., 2006; Moore et al., 2006). Interestingly, both fluorescence

105 parameters may contain signatures of both the nutritional status and taxonomy (Hughes et al.,

106 2018b, 2021; Suggett et al., 2009b), suggesting that it might be possible to establish predictable

107 relationships between FRRf-derived biophysical characteristics and photosynthetic rates within

108 dynamic systems where light, nutrients, and phytoplankton assemblage composition are highly-

109 variable in space and time (Moore et al., 2003).

110 The East China Sea (ECS) is situated in the vicinity of China, South Korea and Japan, and

111 is one of the largest and most productive marginal seas in the world (Chang et al., 2003; Wong et

112 al., 1998). The ECS notably features a complex current system, particularly during summer when

113 it is influenced by both fresh Changjiang Diluted Water (CDW) freshwater discharge and saline

114 Kuroshio saltwater intrusion (Guo et al., 2006; Figure 1A). It is well-documented that

115 phytoplankton biomass, photophysiology and production can vary significantly in response to

116 rapidly-changing gradients of light and nutrients along the coastal to the offshore waters of the

117 ECS (Chen et al., 2004; Gong et al., 2000; Jiang et al., 2014, 2015; Liu et al., 2019; Ning et al.,

118 1988; Yoshikawa & Furuya, 2008). Due to the physical and biological dynamics within the

119 Changjiang estuary and adjacent coastal waters, development of a reliable, high-resolution tool to

120 monitor PP variability in this region would be highly-advantageous.

121 By performing parallel in-situ measurements of net PP and FRR in the Changjiang estuary

122 and adjacent ECS during two summer cruises (Figure 1B), here we develop a generalized additive

123 model (GAM) to predict the net PP data as a function of phytoplankton biomass (Chl-a) and

124 photophysiological parameters which can both be measured with relatively little time and effort.

125 A growing number of research applications are using GAMs to evaluate and predict water

126 environment changes of nutrient, phytoplankton biomass as well as primary productivity (Harding

127 et al., 2016, 2020; Liu et al., 2016; Richards et al., 2013; Testa et al., 2018). Our modeling approach

128 based on GAMs allows for broad-scale retrieval of net PP across the Changjiang estuary and

129 associated coastal waters. Such capability could greatly enhance our understanding of carbon

130 cycling dynamics and long-term changes in ecosystem health within this ecologically important
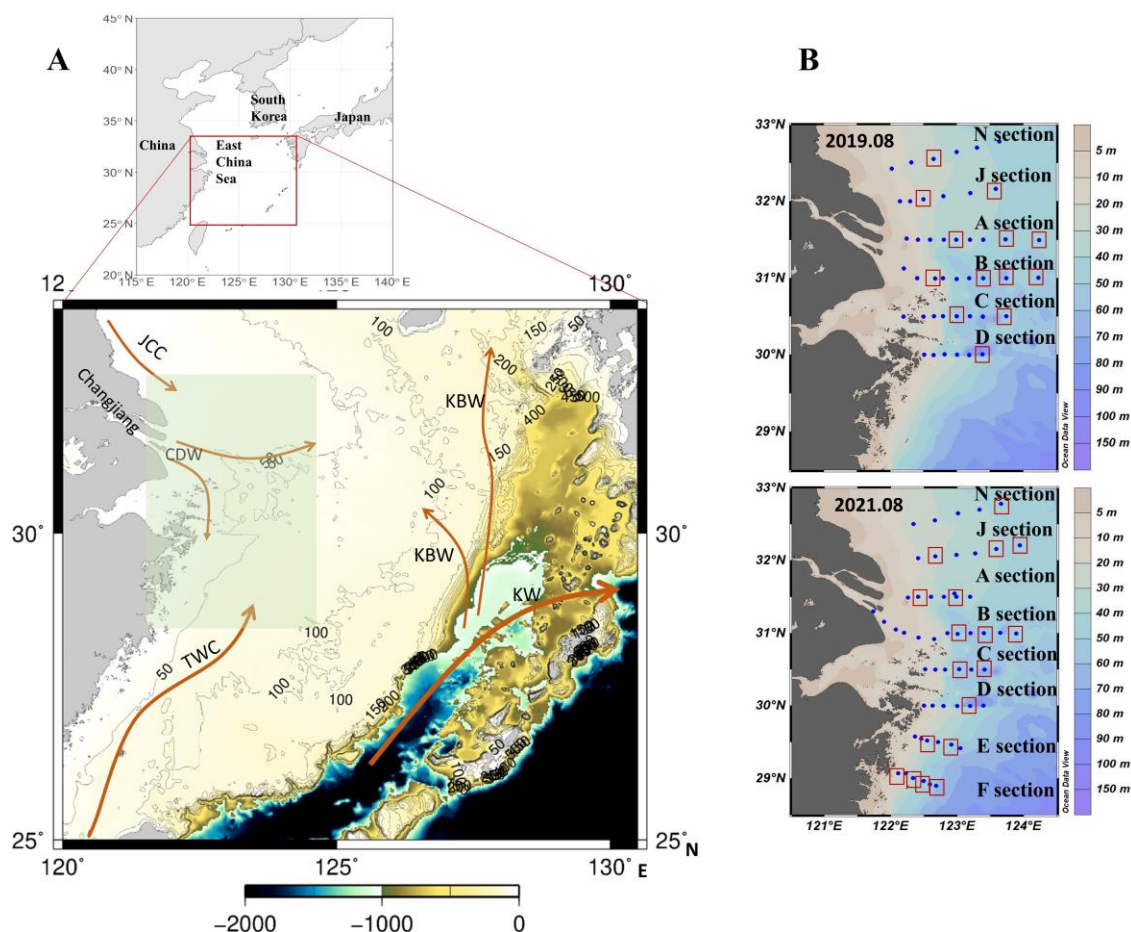
131 region.

132

133 **Figure 1.** (a) Map of the East China Sea (ECS) indicating the main study region (light green shaded

134 area) from which most of our data were collected. The main currents observed during the summer

135 period are also shown: Kuroshio Water (KW), Kuroshio Branch Water (KBW), Taiwan Warm

136 Current (TWC), Jiangsu Coastal Current (JCC) and Changjiang Diluted Water (CDW) (Guo et al.,

137 2006). Light grey lines indicate the isobath. (b) Sampling stations during the summer cruise of

138 2019 and 2021 performed onboard the R/V *Runjiang*. Red squares indicate stations where net

139 primary productivity (PP) data were measured.

140

2 Materials and Methods

2.1 Sample Collection and Physicochemical Properties

Two summer cruises were conducted as a part of the Long-term Observation and Research Plan in the Changjiang Estuary and the Adjacent East China Sea Project (LORCE I&II) from 15th - 25th August 2019, and 15th August − 4th September 2021 (Figure 1). Hydrographic measurements (temperature and salinity) and surface water samples (~1m) were collected using Niskin bottles attached to a rosette sampler that was equipped with a conductivity-temperature-depth (CTD) profiler (Seabird SBE CTD 911). Upper mixed layer depth (MLD) was defined as a density change from the ocean surface of 0.125 sigma units as per Huang & Russell (1994). Nutrient samples were collected from surface waters and filtered using a 0.4 μm polycarbonate membrane filter into 100 mL high-density polyethylene (HDPE) bottles. Ammonium–nitrogen (NH_4^+-N) was immediately measured onboard via indophenol blue spectrophotometric method (Grasshoff et al., 1999), while samples for nitrate + nitrite (NO_3^- + NO_2^-) and phosphate (PO_4^{3-}) analyses were stored at –20 °C for later analysis using an automated nutrient analyzer (SEAL Analytical, Germany). Dissolved inorganic nitrogen (DIN) was determined as the sum of NH_4^+, NO_3^- and NO_2^-.

2.2 Chl-a and ^{13}C uptake-based net primary productivity

Chlorophyll-a concentrations were determined from 100 mL seawater samples filtered through GF/F filters, using a pre-calibrated fluorometer (Trilogy, Turner Design, USA) following the non-acidification method (Welschmeyer, 1994). GF/F filters were soaked in 90% Acetone and pigments were extracted for 24 h at -20°C in darkness before subsequent fluorometric evaluation.^{13}C uptake experiments were carried out via 24 h on-deck bottle incubations. Seawater was pre-filtered through 200-μm mesh to remove zooplankton grazers and then used to fill three 500 mL polycarbonate bottles.^{13}C-labeled sodium bicarbonate (99 atom %; $NaH^{13}CO_3$, CIL, USA) was added to each bottle where the final ^{13}C atom % of total dissolved inorganic carbon was ca. 10 % of that in the ambient seawater (Hama et al., 1983). Samples were placed in a shipboard incubator connected to the ship's underway seawater system to control incubation temperature. The incubator was shaded with neutral density filter to achieve 50% transmission of measured surface irradiance. After 24 h, all samples were filtered through 25mm pre-combusted GF/F filters (450 °C, 6 h) and stored at –80 °C until further analysis. Filter samples were then vacuum-dried after exposure to fumes of HCl to remove excess particulate inorganic carbon. The concentration

171   of particulate organic carbon (POC) and the isotopic ratio of ^{13}C and ^{12}C (^{13}C atomic %) on the

172   filters were then determined using an isotope ratio mass spectrometer (Delta^{PLUS}, Thermo Fisher

173   Scientific, USA) equipped with an elemental analyzer (EA 1110, CE Instruments). Finally,

174   volumetric C-fixation rates were calculated according to Hama et al. (1983) (Eq. 1):

175

176    $$P^C = \frac{POC \times (a_{is} - a_{ns})}{t \times (a_{ic} - a_{ns})} \tag{1}$$

177   where P^C is the net carbon fixation rate (mgC m^{-3} d^{-1}), t is the time of incubation in days

178   (for this study, 1d). a_{is} is the atomic% of ^{13}C in the incubated sample, a_{ns} is the atomic% of ^{13}C

179   in the natural sample, and a_{ic} is the atomic% of ^{13}C in the total inorganic C. Chl-a specific primary

180   productivity (P_B^C, mgC [mgChl-a]$^{-1}$ d^{-1}) was calculated as P^C normalized to measured Chl-a

181   concentration.

182   2.3 Fast Repetition Rate (FRR) fluorometry

183   Variable chlorophyll fluorescence was measured using a Fast Repetition Rate (FRR)

184   fluorometer (FastOcean) integrated with a FastAct laboratory base unit system (Act2, Chelsea

185   Technologies Ltd, London, United Kingdom). Water samples collected during daytime (8:00 –

186   17:00) were measured after 30 min dark adaptation to relax non-photochemical quenching (NPQ)

187   processes, and measurements for all samples were completed inside an hour. FRR fluorometry

188   measurements were corrected for blank (or baseline) fluorescence using 0.2 µm filtrates (Cullen

189   & Davis, 2003; Schuback et al. 2021). Since diatoms and dinoflagellates are known to dominate

190   phytoplankton assemblages in the study area (Jiang et al., 2014, 2015；Yang et al., 2014), the blue

191   (447 nm) excitation band was solely used for photophsyiological measurements of all samples

192   (e.g., Zhu et al., 2017, 2022). The FRR fluorometer was programmed to deliver a single-turnover

193   protocol with a saturation phase comprising 100 flashlets on a 2 µs pitch, followed by a relaxation

194   phase comprising of 50 flashlets on a 150 µs pitch. Each FRRf acquisition was subsequently fitted

195   to the KPF model of Kolber et al. (1998) to derive the minimum fluorescence yield (F_o), maximum

196   fluorescence yield (F_m), functional absorption cross section of PSII ($\sigma_{\square\square\square\square}^{447}$), and maximum

197   photochemical efficiency of PSII (F_v/F_m, where $F_v = F_m - F_o$).

198   2.4 Statistical Analyses

199   Correlations between the independent parameters were analyzed using Spearman's rank

200 order correlation coefficient. Stepwise regression was used to examine the contribution of

201 physicochemical variables in explaining variance of net PP (Probability of F to enter $<= 0.05$) and

202 to develop a multiple linear model for net PP estimation. The comparion of mean values of grouped

203 samples was tested by one-way non-parametric ANOVA (Kruskal-Wallis test). In addition, a

204 Generalized Additive Modelling (GAM) approach was proposed for modeling of phytoplankton

205 PP to meet current and future assessment needs. The mathematical formulation of a typical GAM

206 is presented in Eq.2:

207        $$g(E[Y]) = \mu + f_1(x_1) + f_2(x_2) + \cdots + f_n(x_n) \qquad\qquad (2)$$

208   where a function $g()$ is applied to the expected value (E) of the dependent variable Y (in

209 this case, Net PP). μ is the modeled intercept. $f()$ is the smoothing function of the independent

210 variables $x_1, x_2, \dots x_n$. Analyses were implemented using the mgcViz package in R (Fasiolo et al,

211 2018), where cubic regression spline was used to optimize the smoothing functions, and correlation

212 coefficient (R^2), root mean square error (RMSE) and Akaike information criterion (AIC) were used

213 to evaluate model explanatory power, goodness of fit, and parsimony respectively. Due to the

214 small sample size, the RMSE between actual values and predicted values was calculated using the

215 Leave-One-Out Cross-Validation (LOOCV) procedure (Yada & Shukla, 2016).

216   All statistical analyses and curve fitting were performed using the open-source statistical

217 software R (Version 3.6.1, R Core Team 2019). Data were visualized using GMT 4, Ocean Data

218 View 5 (Schlitzer, 2018) and R Studio software.

219 **3 Results**

220   3.1 Hydrography and Chlorophyll-a biomass

221   Sampling while transiting from the Changjiang mouth to offshore, revealed a strong

222 gradient of physico-biological conditions present in ECS surface waters during summer (Table 1;

223 Figure 2). High sea surface temperatures (SST) and low sea surface salinity (SSS) values were

224 observed along Changjiang mouth sections (section A and B, Figure 2A, B, C, D). Highest Chl-a

225 concentrations were observed in the centre of the study area along the 123°E longitude, as well as

226 in the coastal upwelling zone known as Zhoushan upwelling (Figure 2B). Relatively low Chl-a

227 values were measured in both coastal and offshore waters (Figure 2E, F). Notably, a diatom bloom

228   (where a bloom is defined as a Chl-a concentration > 30 µg L^{-1}) occurred outside of the Changjiang

229   mouth during the 2021 cruise (Figure 2F).

230   Biophysical variables were notably different observed between two cruises, likely caused

231   by the variations of Changjiang runoff at the times of sampling. Averaged runoff (between August

232   15th - 31st) from the Changjiang river measured at the Datong hydrological station, was 39,152 ±

233   3860 m^{3}s^{-1} in 2010 but was ~10% higher in 2021 at 43,341 ± 1448 m^3 s^{-1}. Consequently, CDW

234   (featured as low salinity water) extended further east in 2021 compared to 2019 (Figure 2C, D).

235   Area-averaged nutrient concentrations were also higher in 2021, with DIN and PO$_4^{3-}$ values of 22.2

236   ± 26.3 µmol L^{-1} and 0.46 ± 0.51 µmol L^{-1} respectively, compared to 19.3 ± 18.8 and 0.32 ± 0.39

237   µmol L^{-1} in 2019. In conjunction with higher nutrient levels, the average Chl-a concentration in

238   2021 was approximately twice that of 2019 (6.14 ± 6.88 µg L^{-1} vs. 2.71 ± 2.61 µg L^{-1}) and also

239   spanned a much wider range (0.27 - 38.4 µg L^{-1}) compared to 2019 (0.18 to 11.1 µg L^{-1}; Figure

240   2E, F).

241

242   **Table 1.** Geographical locations and surface values of physico-chemical and biological variables
243   measured at stations where primary productivity (PP) incubations were performed in the
244   Changjiang estuary and adjacent East China Sea during two summer cruises in 2019 and 2021.
245   Lon: longitude, Lat:latitude, Temp: temperature (°C), Sal: salinity, MLD: mixed layer depth (m),
246   DIN: dissolved inorganic nitrogen (µmol L^{-1}), Chl-a: chlorophyll a (µg L^{-1}). BLD represents those
247   samples below the limit of detection, and N/A = data not available.
248

Station	Lon	Lat	Temp	Sal	MLD	DIN	PO$_4^{3-}$	Chl-a
2019-N3	122.65	32.5	26.0	29.7	5	10.04	0.05	4.08
2019-J3	122.5	32.0	28.5	25.4	3	17.9	0.05	0.86
2019-J6	123.58	32.2	27.8	30.1	10	5.2	BLD	1.16
2019-A5	122.99	31.5	28.5	23.0	5	17.1	BLD	2.44
2019-A8	123.73	31.5	28.8	30.9	8	1.35	BLD	0.64
2019-A9	124.24	31.5	28.9	30.3	16	0.8	BLD	0.47

2019-B6	122.67	31.0	7.1	22.8	2	34.8	0.55	2.1
2019-B10	123.40	31.0	28.2	33.5	10	0.23	BLD	0.57
2019-B11	123.75	31.0	28.8	31.1	11	0.99	BLD	0.45
2019-B12	124.23	31.0	28.6	30.8	10	0.55	BLD	0.40
2019-C5	123.0	30.5	28.1	30.4	5	2.0	BLD	0.61
2019-C8	123.75	30.5	28.9	33.5	8	2.5	BLD	0.21
2019-D6	123.38	30.0	28.9	32.2	6	N/A	N/A	0.18
2021-N6	123.66	32.8	27.5	30.0	10	N/A	N/A	1.61
2021-J2	122.41	32.0	28.3	26.9	8	28.1	0.49	4.52
2021-J5	123.3	32.1	28.4	31.6	10	1.9	BLD	0.87
2021-J6	123.6	32.1	28.0	32.6	9	0.93	0.05	1.72
2021-A2	122.4	31.5	27.9	11.7	4	16.5	0.67	3.84
2021-A5	123	31.5	29.1	15.6	5	32.7	0.11	38.4
2021-B8	123	31	28.3	23.2	5	23.8	0.16	21.2
2021-B10	123.4	31.0	28.5	26.7	10	8.14	0.07	4.35
2021-B12	123.9	31.0	28.5	29.6	14	0.14	0.05	1.4
2021-C5	123.0	30.5	27.4	27.5	5	1.0	0.09	18.1
2021-C7	123.4	30.5	28.1	31.7	17	N/A	N/A	0.57

2021-D5	123.2	30.0	28.4	31.2	6	0.48	0.06	1.05
2021-E3	122.5	29.5	26.9	26.9	5	14.7	0.12	8.36
2021-E5	122.9	29.4	28.7	30.8	7	0.46	0.17	2.34
2021-F1	122.1	29.1	27.7	28.0	5	25.6	1.01	1.62
2021-F3	122.3	29.0	26.7	26.2	6	20.5	0.33	15.01
2021-F4	122.5	28.9	28.0	31.3	11	1.27	0.07	3.96
2021-F6	122.7	28.9	28.1	30.7	11	0.67	0.08	5.26

249

250

251
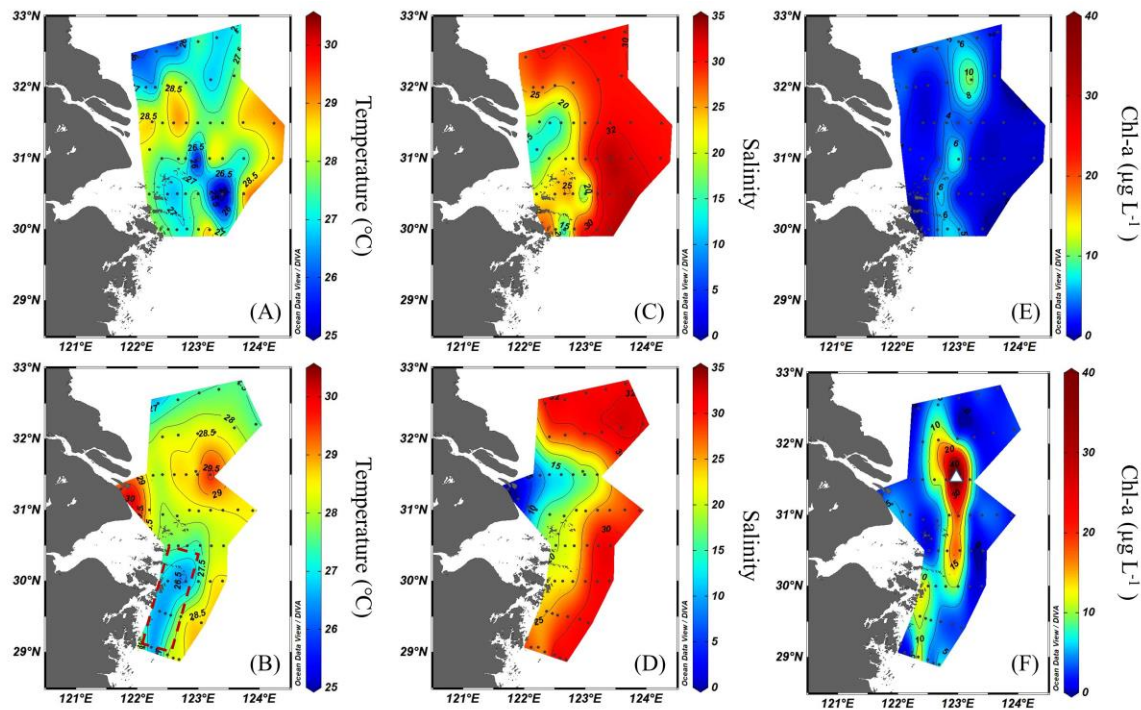
Figure 2. Spatial variability in temperature (°C), salinity (PSU) and Chlorophyll-*a* (Chl-a, µg L^{-1}) in 2019 (a, c, e) and 2021 (b, d, f) cruise. The red dashed box in (b) indicates the upwelling zone. The white triangle in (f) indicates the location of an observed diatom bloom.

255   3.2 Phytoplankton photophysiology

256   Surface F_v/F_m and σ_{PSII}^{447} values showed wide ranges and significant variability when all

257   data were pooled (Figure 3). F_v/F_m ranged from 0.14 - 0.61, averaging 0.45 ± 0.06 over the study

258   area. Overall, higher values of F_v/F_m (> 0.5) were mostly associated with high Chl-a, while low

259   F_v/F_m values (< 0.4) were mostly observed in the offshore waters characterized by low

260   phytoplankton biomass (Figure 3A, B). There were however some notable exceptions where

261   F_v/F_m values > 0.5 were observed in several offshore stations that also exhibited low Chl-a

262   concentrations (e.g., B12 in Figure 3A and J6, C7 in Figure 3B), likely reflecting the different

263   photosynthetic strategies used by phytoplankton to cope with this varied environment. Surface

264   σ_{PSII}^{447} values ranged from 2.96 - 7.46 nm^2 PSII^{-1} and exhibited a clear spatial trend (Figure 3C, D).

265   Generally, σ_{PSII}^{447} values were low in the Changjiang month and adjacent waters (< 4.5 nm^2 PSII^{-1})

266   and increased with distance offshore (Figure 3C, D). No significant correlation was found between

267   F_v/F_m and σ_{PSII}^{447} ($r = -0.22$, n = 80, $p = 0.053$). Meanwhile, F_o was found significantly and

268   positively correlated with Chl-a (Spearman, $r = 0.818$, n = 80; $p < 0.001$; Supplementary Figure

269   S1).

270   While comparing phytoplankton physiological features between datasets of 2019 and 2021,

271   it was notable that both the highest and lowest F_v/F_m and σ_{PSII}^{447} values were observed in 2021,

272   perhaps reflecting more drastic environmental changes during the cruise period in this year. The

273   mean F_v/F_m value was almost identical in both years (0.45 ± 0.04 compared to 0.46 ± 0.08 in 2019

274   and 2021, respectively), while σ_{PSII}^{447} was on average ~10% lower in 2021 (5.01 ± 1.07 vs. $5.45 \pm$

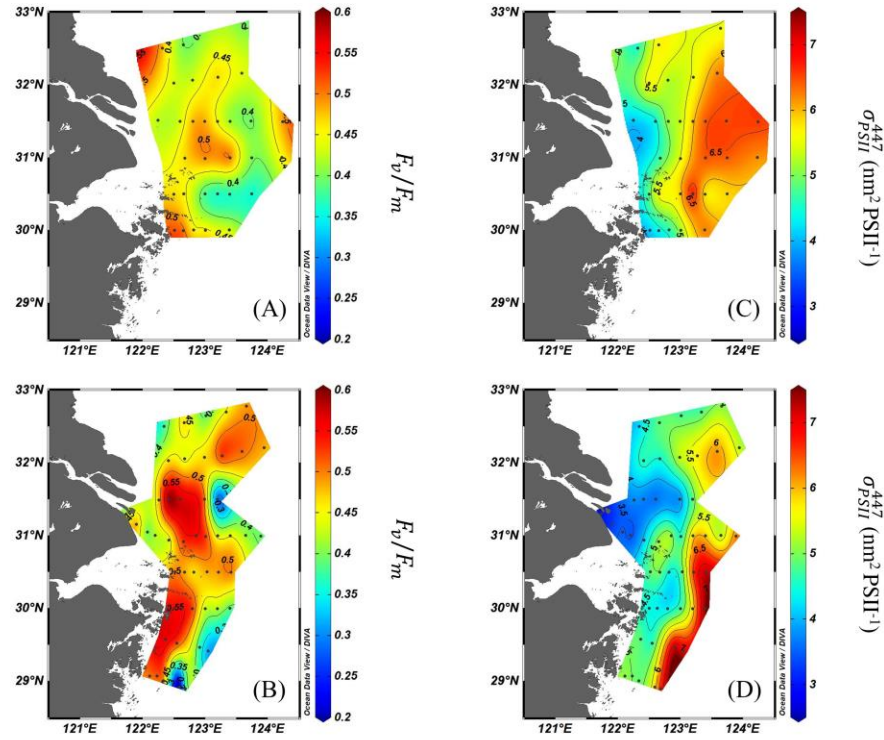275 0.77 nm^2 PSII^{-1}) (ANOVA, $p = 0.028$).

276

Figure 3. Spatial variability in photophysiological parameters: the maximum quantum yield of Photosystem II (PSII), F_v/F_m (unitless) and the functional absorption cross-section of PSII, σ_{PSII}^{447} (nm^2 PSII^{-1}) during the 2019 (a, c) and 2021 (b, d) cruises.

280   3.3 Phytoplankton Primary productivity (PP)

281   A total of 31 ^{13}C-incubations were performed over both years, with surface carbon uptake

282 rates (P^C) spanning several orders of magnitude, ranging between 6.0 – 1,679 mgC m^{-3} d^{-1}. Higher

283 PP values were generally found in coastal waters, while the majority of lower PP values were

284 measured at offshore stations (**Figure 4A, B**). Interestingly, the spatial distribution of Chl-a

285 normalized carbon uptake rates (P_B^C) differed from that of P^C, where high P_B^C values were

286 measured in both coastal and offshore waters (**Figure 4C, D**), likely reflecting the interactive

287 effects of different environmental factors (e.g., nutrient, light, mixing layer depth, etc.) and

288 phytoplankton community structure on the efficiency of phytoplankton C-uptake (e.g., Firme et al.

289 2023). Similar to the observed trend in Chl-a distribution, a wider range and higher average net PP

290 values were observed in 2021 (74.3 - 1,679 mgC m^{-3} d^{-1}, mean: 527 ± 511 mgC m^{-3} d^{-1}) compared

291 to 2019 (6.0 - 260 mg C m^{-3} d^{-1}, mean: 66.0 ± 68.5 mg C m^{-3} d^{-1}). Average P_B^C was ~1.5 times

292 higher in 2021 than 2019 (97.7 ± 68.1 vs. 69.5 ± 48.5 mgC [mg Chl-a]$^{-1}$ d^{-1}). Therefore, it appeared

293   that the higher PP values observed for 2021 were likely driven by both higher Chl-a concentrations

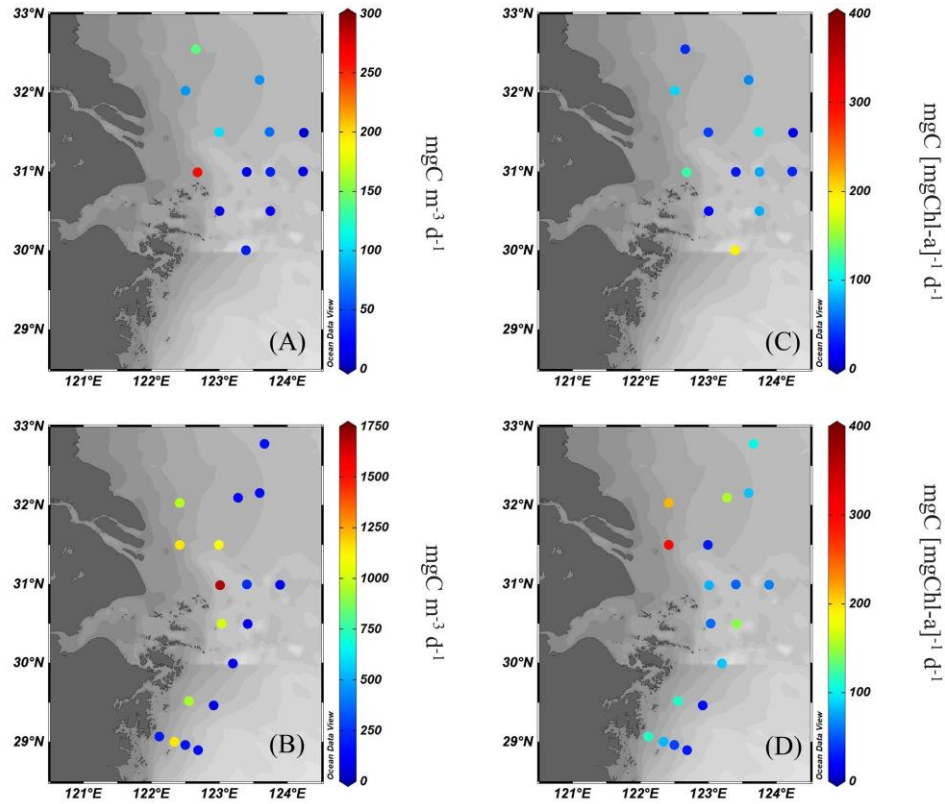294   and greater phytoplankton C-uptake efficiency.

296   **Figure 4.** Spatial variability in surface net carbon fixation rates, P^C (mgC m^{-3} d^{-1}) and Chlorophyll-
297   a (Chl-a) specific carbon fixation rates, P_B^C (mgC [mgChl-a]$^{-1}$ d^{-1}) during the 2019 (a, c) and 2021
298   (b, d) cruises.

299   3.4 Net PP Modelling

300   Spearman rank correlation analysis between net PP and various physical, biological and

301   physiological variables revealed that salinity, F_v/F_m, σ_{PSII}^{447} and Chl-a were all correlated with net

302   PP (Table 2), with Chl-a and σ_{PSII}^{447} exhibiting the highest correlation coefficients ($r = 0.881$ and r

303    $= -0.759$ respectively, $p < 0.001$). Stepwise linear regression (SLR) analysis further confirmed that

304   Chl-a and σ_{PSII}^{447} were key predictor variables of PP variability. While σ_{PSII}^{447} alone explained the

305   most variability of NPP (61%), adding Chl-a further improved the predictive power of the model,

306   increasing R^2 to 0.73 ($p < 0.001$, Table 3). The multiple linear model ($P^C = -a \times \sigma_{PSII}^{447} +$

307    $b \times Chla + c$) yielded an RMSE of 248.7 mgC m^{-3} d^{-1} (Table 3).

308

309

310

311 **Table 2.** Spearman rank analysis for correlations between net primary productivity (P^C, mg C m^{-3} d^{-1}) and environmental variables (temperature, salinity) and photophsyiological parameters (Photosystem II (PSII) maximum quantum yield [F_v/F_m], the functional absorption cross-section of PSII [σ_{PSII}^{447}, nm^2 PSII^{-1}]) and Chlorophyll-a concentration (Chl-a, µg L^{-1})

		Temp	Sal	F_v/F_m	σ_{PSII}^{447}	Chl-a
P^C	r	0.186	0.451*	0.596*	**-0.759****	**0.881****
	p value	0.318	0.011	0.01	0.000	0.000
	n	31	31	30	30	31

315
316 * and ** denotes statistical significance at $p < 0.05$ and 0.01 respectively
317

318

319 **Table 3.** Influence of various physiological and biological variable on carbon fixation rates, P^C,
320 estimated by stepwise linear regression.

No. of predictor variables	Variables	R^2	RMSE
1	σ_{PSII}^{447}	0.61	/
2*	σ_{PSII}^{447}, **Chl-a**	**0.73**	**248.7**

321
322 *$P^C = -a \times \sigma_{PSII}^{447} + b \times Chla + c$, where $a = 246.75, b = 25.77, c = 1611.2$
323

324

325   To account for the potential non-linear impacts of σ_{PSII}^{447} and Chl-a on P^C (Figure 5), a
326 Generalized Additive Model (GAM) approach was applied to develop a predictive model of net
327 PP including the following two predictors: ($P^C \sim$ s(σ_{PSII}^{447}) + s(Chl-a)). Seven GAM sub-models
328 based on different combinations of knots number (k) were tested (Table 4), with sub-model GAM6
329 found to be best-performing model (Table 4). The RMSE of GAM was smaller than that of the
330 multiple linear model (144.2 vs. 248.7 mgC m^{-3}d^{-1}), indicating net PP in this study area could be
331 better predicted by its nonlinear relationship with Chl-a and σ_{PSII}^{447} (see Figure 6 for response plots
332 of best-fitting GAM with both σ_{PSII}^{447} and Chl-a). Overall, GAMs predicted similar distribution
333 patterns of surface net PP to observed values, with high rates mainly distributed in the coastal areas,

334   and relatively low rates tended to occur in the offshore waters (R^2 = 0.94, n = 30; $p < 0.001$;
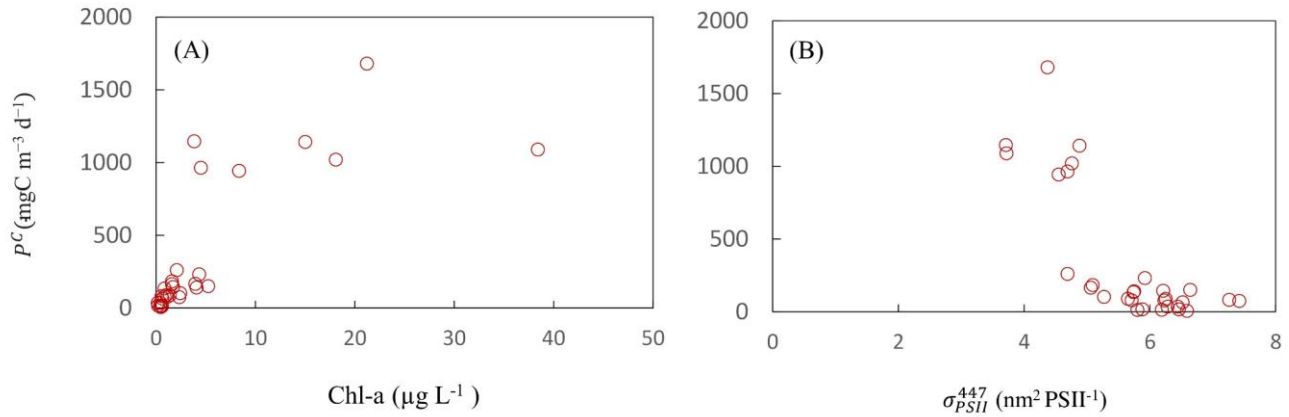
335   Supplementary Figure S2, Figure 7).

336

3__

338   **Figure 5.** Scatter plots of net primary productivity, P^C (mgC m^{-3} d^{-1}) against (a) the functional

339   absorption cross-section of PSII, σ_{PSII}^{447} (nm^2 PSII^{-1}) and (b) Chl-a concentration (μg L^{-1}).

340

341

342

343

344

345

346

347

348

349

350

351

352

353

354

355

356 **Table 4.** Statistics for generalized additive models (GAM) of net primary productivity (PP) in the
357 Changjiang estuary and East China Sea using predictor variables (Table 3). Submodels GAM1 to
358 GAM7 involve different combinations of k for σ_{PSII}^{447} and Chl-a, respectively; AIC =Akaike
359 information criterion; RMSE =root mean square error.
360

361

No. of GAM submodel	predictor variables	k	R^2	AIC	RMSE
GAM 1	σ_{PSII}^{447}, Chl-a	3, 3	0.902	390.7	165.0
GAM 2	σ_{PSII}^{447}, Chl-a	4, 3	0.906	389.9	161.7
GAM 3	σ_{PSII}^{447}, Chl-a	3, 4	0.929	381.8	141.3
GAM 4	σ_{PSII}^{447}, Chl-a	4, 4	0.929	382.16	143.7
GAM 5	σ_{PSII}^{447}, Chl-a	5, 4	0.928	382.8	144.7
GAM 6*	**σ_{PSII}^{447}, Chl-a**	**4, 5**	**0.933**	**380.42**	**144.2**
GAM 7	σ_{PSII}^{447}, Chl-a	5, 5	0.932	381.3	153.4

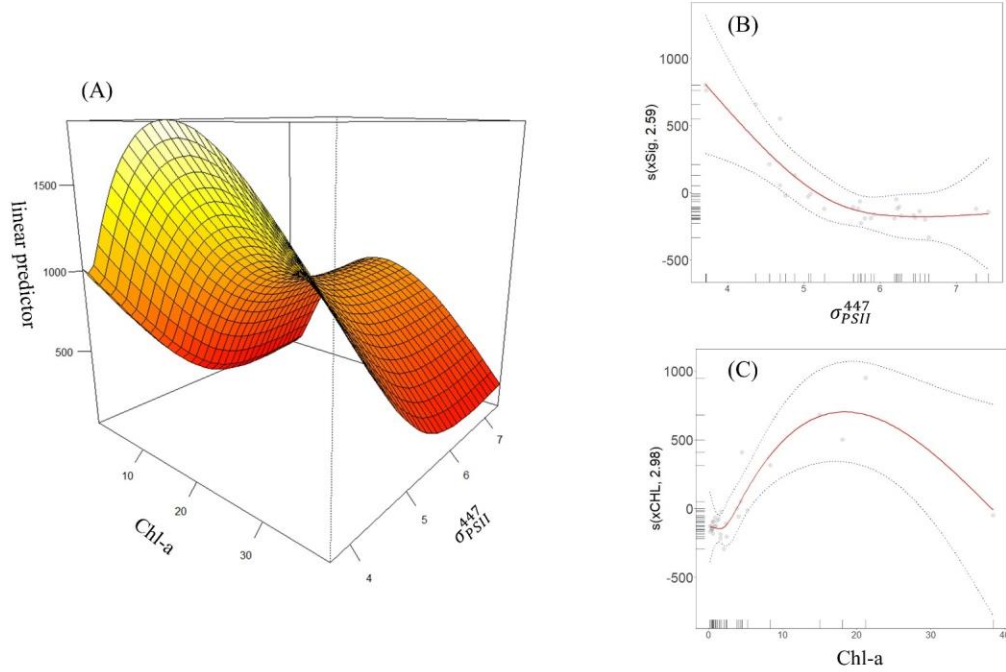362 * represents the best-fitting GAM
363

364

Figure 6. Interaction effects of the optimal Generalized Additive Model (GAM), showing (a) significant interaction between σ_{PSII}^{447} and Chl-a. (b-c) GAM results describing P^C (mgC m^{-3} d^{-1}) variability with σ_{PSII}^{447} (nm^2 PSII^{-1}) and Chl-a concentration (µg L^{-1}).
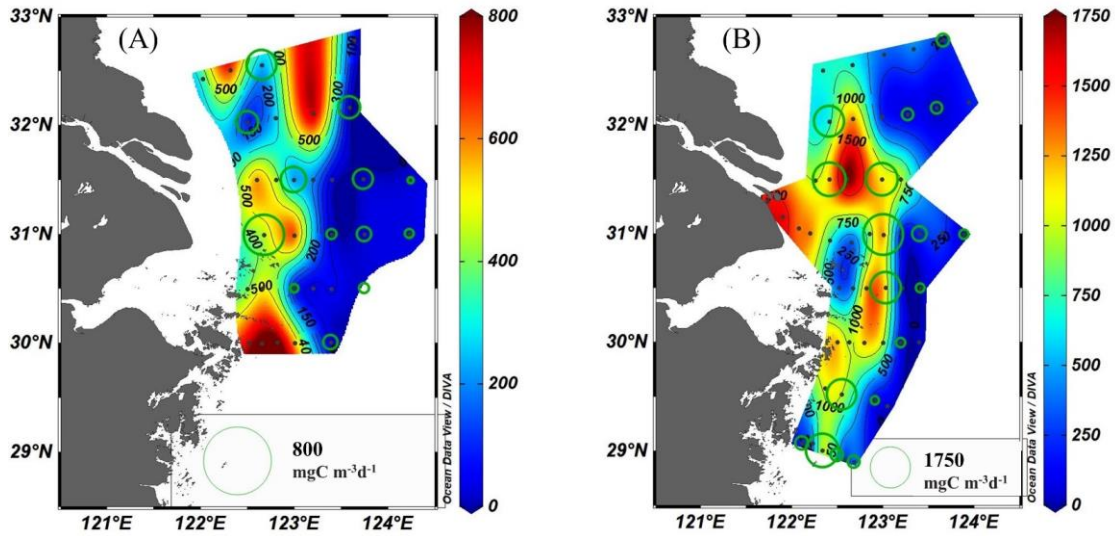
368

Figure 7. Overlaid plots between observed (sized dots) and predicted net primary productivity (PP) (based on the best-fitting Generalized Additive Model [GAM] shown in Table 4) during (a) 2019 and (b) 2021 summer cruises.

4 Discussion

Assessing carbon cycling in dynamic coastal systems such as the Changjiang estuary and adjacent ECS is challenging due to the low sampling resolution of conventional, incubation-based methods. Here, we developed an empirical model to assess PP at high-resolution. We demonstrate for the first time how knowledge of Chl-a biomass and phytoplankton photophysiology can be used to predict PP across the strong environmental gradient present in this region during summertime. Importantly, unlike previous work which has estimated C-uptake rates from FRR-derived measurements (ETRs) by calculating (or assuming) K_C and n_{PSII} values (e.g., Hancke et al., 2015; Schuback et al., 2015; 2017; Wei et al., 2019; Zhu et al., 2015, 2017), our approach allows for retrieval of PP estimates without knowledge or assumption of either, or both, parameters which are difficult to measure in nature. We discuss insights gleaned from application of FRR fluorometry to this study area, and how our GAM modelling approach provides a high-resolution solution to rapidly assess regional PP at and carbon cycling dynamics.

4.1 Insights into phytoplankton photophysiology

During summer, the spatial distribution of Chl-a within the Changjiang estuary and nearby East China Sea is mainly influenced by the equilibrium effects of light availability and nutrient supply, shaping a so-called "sandwich" pattern (Ning et al., 1988; Li et al., 2021). Specifically, Chl-a values were mostly higher along the boundaries of Changjiang plume front compared to either coastal and offshore waters (Li et al., 2021, Figure 2E, F). Overall, a similar spatial pattern was observed for F_v/F_m values when all data were pooled, revealing a significant positive correlation between these two parameters (Spearman's Rank, $r = 0.31$, n = 76, $p = 0.006$) - as also observed in previous studies (Gutiérrez-Rodríguez et al., 2020; Liu et al., 2022; Zhu et al., 2019). Several factors are thought to control F_v/F_m including the light environment, nutrient availability, and the taxonomic composition of the phytoplankton community itself (Suggett et al., 2009b). Decreases in F_v/F_m are commonly observed in nutrient-starved phytoplankton (Geider et al., 1993, 1998a, b; Parkhill et al., 2001) and may explain the low F_v/F_m values recorded at offshore stations in this study where nutrient availability was low (Figure 3A, B). Meanwhile, at the Changjiang mouth where nutrient levels are elevated - and presumably not limiting for phytoplankton growth – the lower F_v/F_m values are likely explained by another factor. While the presence of smaller phytoplankton cells can contribute to lower F_v/F_m values (Suggett et al. 2009b), size-fractionated Chl-a analysis found that our sampling sites near the Changjiang mouth were actually dominated

404   by phytoplankton cells >10 μm (~90%, data not shown) and thus taxonomy is unlikely to account

405   for the low F_v/F_m values observed here. Due to increased stratification and shallow mixed layer at

406   this location, it is likely that low F_v/F_m values are instead caused by PSII photoinactivation

407   (Osmond, 1994; Moore et al., 2006; Fisher et al. 2020) - which occurs when phytoplankton are

408   exposed to higher light levels for longer periods – and manifests as reduced PSII photochemical

409   efficiency (Fisher et al. 2020). Conversely, relatively high F_v/F_m values were also found at several

410   offshore stations where nutrients were likely limiting (DIN < 0.5 μM, PO_4^{3-} < 0.05 μM; Figure 3A,

411   B). This result is not surprising because it is consistent with the interpretation that phytoplankton

412   cells can maintain F_v/F_m values under steady-state macronutrient limitation, rather than starvation

413   (MacIntyre et al., 1997; Parkhill et al., 2001; Behrenfeld et al., 2006; Kruskopf & Flynn, 2006;

414   Moore et al., 2008; Schrader et al., 2011).

415   In addition to light spectrum dependence, changes in σ_{PSII} are typically related to the

416   photoacclimational status, cellular nutrient status and/or taxonomic shifts in the phytoplankton

417   assemblage (Moore et al., 2006; Suggett et al., 2009b). While σ_{PSII} is expected to increase as cell

418   size declines (see Suggett et al., 2009b), we observed no correlation between σ_{PSII}^{447} and proportion

419   of Chl-a >10 μm (Spearman, $p = 0.09$; data not shown), further reinforcing the notion that

420   phytoplankton community structure and composition is unlikely the primary driver of

421   physiological variability in our dataset. Higher values of σ_{PSII}^{447} measured in the nutrient-poor

422   offshore waters are consistent with previous studies showing that σ_{PSII} increases with decreasing

423   nutrient supply (Kolber et al., 1988; Berges et al., 1996; Moore et al., 2003, 2005; Kulk et al.,

424   2018). Meanwhile, the light environment experienced by phytoplankton from nearshore to

425   offshore waters in the Changjiang estuary is likely to vary considerably with changing upper

426   MLDs (Table 1). Typically, when experiencing an increase in growth irradiance, phytoplankton

427   reduce their light harvesting capacity by decreasing σ_{PSII} to avoid photodamage (Falkowski et al.,

428   1981). Conversely, phytoplankton cells acclimated to low light usually increase the number and/or

429   the 'size' of their photosynthetic units, which also resulting in an increased PSII functional cross-

430   section (σ_{PSII}) (Moore et al., 2006; Six et al., 2008). Unsurprisingly, higher σ_{PSII}^{447} values were

431   mostly measured in deeper mixed offshore waters – where a larger PSII functional cross-section

432   is conducive to increased light absorption per reaction center II (RCII), and is clearly advantageous

433   at the low irradiance levels characteristic of this environment (Kolber et al., 1988; McKew et al.,

434   2013; Schuback et al., 2017).

435   4.2 Controls of phytoplankton primary productivity

436   Surface PP values exhibited remarkable variability, ranging from ~6 - 1600 mgC m^{-3} d^{-1}

437   over the two summer sampling campaigns. Overall, phytoplankton PP and Chl-a were positively

438   correlated (Table 2), reflecting that phytoplankton biomass is a key driver of C-uptake rates.

439   However, pooling of the data revealed a decoupling between these two parameters, suggesting a

440   maximum level of PP exists, beyond which further increase in Chl-a do not necessarily translate

441   to increased production (Figure 5A). An apparent decoupling was also observed in the spatial

442   distributions of Chl-a and PP, with high PP observed in coastal waters despite relatively low Chl-

443   a (Figure 2, 4). Such a decoupling between Chl-a and PP is consistent with previous observations

444   in the ECS that attributed this phenomenon to grazing pressure by microzooplankton (Liu et al.,

445   2019). It is well-known that Chl-a concentrations are extremely plastic, with measured changes

446   arising from light-driven (photoacclimation) and nutrient-driven physiological responses, which

447   are not necessarily indicative of proportional changes in productivity (Behrenfeld et al., 2016; Liu

448   et al., 2019). Previous laboratory studies of microalgal cultures have found a strong increase in the

449   carbon-to-chlorophyll ratio (C:Chl-a) with increasing growth irradiance, i.e., where phytoplankton

450   cells become less pigmented (Laws & Bannister, 1980; Geider et al., 1987, 1998a). Thus,

451   according to traditional photoacclimation models, when mixing is shallow and light is saturating

452   (e.g., as in the Changjiang mouth, Zhu et al., 2009), less Chl-a is required to sustain a given

453   production rate (Behrenfeld et al., 2016) – and likely explains the spatial uncoupling of

454   phytoplankton Chl-a and productivity observed in this study.

455   Nutrient-driven physiological responses, which also lead to variations in production rates

456   per unit Chl-a could also explain the high production rate yet low Chl-a values sometimes observed

457   in this study. Declines of photosynthetic rates normalized to Chl-a, P_B^C in oligotrophic subtropical

458   gyres is presumably due to nutrient limitation (Behrenfeld & Falkowski, 1997). Marañón et al.

459   (2003) also proposed the existence of nutrient-dependent changes in photosynthetic performance,

460   demonstrating a positive correlation between nutrient supply rates and Chl-a-normalized C-

461   fixation rates. Thus, it is plausible to suggest that higher production rates per Chl-a could be

462   sustained in the coastal water and Changjing mouth with enhanced nutrient supply (Figure 4, 7).

463   On the other hand, however, a shift in bloom stages associated with depleted nutrient

464   concentrations (Table 1) is likely to decrease P_B^C and thus may contribute to inconsistent observed

465   trends for net PP and Chl-a (Figure 5A, Waga et al., 2022).

466   4.3 Relationship between primary productivity and PSII functional absorption cross
467   section

468   We found a strong negative correlation between σ_{PSII}^{447} and net PP in the this study (Table
469 2, Figure 5B), suggesting σ_{PSII}^{447} and net PP likely co-varied as a result of physiological and/or
470 taxonomic responses to changing environmental conditions in this dynamic sampling area (Moore
471 et al., 2003). Under nutrient limitation, phytoplankton species tend to reduce the abundance of the
472 key D1 protein associated with PSII repair, together with CP43 and CP47, which leads to an
473 increase in σ_{PSII}. Meanwhile, the increased turnover of D1 under nutrient limitation could lead to
474 a reduction in the steady state level of the proteins, which consequently decreased photochemical
475 energy conversion efficiency and phytoplankton growth rates (Greene et al., 1992; Kolber et al.,
476 1988). Upon relief of nutrient deficiency, reduction in σ_{PSII} associated with increased D1 may be
477 apparent in coastal waters where growth rates and primary productivity of phytoplankton are
478 higher. In contrast, under light-limited systems, all PSII traps appear to be fully functional which
479 increase the σ_{PSII} (Kolber et al., 1988). With increasing light, surplus energy supply relative to
480 metabolic demand stimulates a decrease in σ_{PSII} (Huner et al., 1998). Whilst the major factor
481 driving the co-variation of σ_{PSII} and net PP in our study remains unclear, Suggett et al (2009b)
482 suggested that σ_{PSII} is less sensitive to nutrient limitation and thus the change in light availability
483 might outweigh the potential influence of nutrient limitation upon PSII functioning.

484   Along with changes driven by nutrient and light availability, σ_{PSII} and PSII efficiency also
485 appears to vary across algal taxa. Diatoms and larger phytoplankton are generally characterized by
486 lower σ_{PSII} values, whereas smaller phytoplankton or dinoflagellates and nanoflagellates exhibit
487 relatively larger σ_{PSII} values (Suggett et al., 2009b). Furthermore, increased photosynthetic
488 efficiency and growth rates have also been observed for larger phytoplankton under nutrient-
489 replete conditions, which may explain higher PSII photochemical efficiency observed in certain
490 phytoplankton taxa such as diatoms (Cermeño et al., 2005). In summary, NPP and σ_{PSII} are
491 unlikely to vary independently but as a result of some common physiological/ecological
492 mechanism (Moore et al., 2003).

493   Regardless of the underlying cause, the relationship between σ_{PSII} and NPP provides the
494 opportunity of investigating changes in productivity at high resolution via FRR fluorometry in
495 dynamic systems. However, with the decreasing of σ_{PSII}^{447}, the non-linear increasing of net PP may
496 limit the power of σ_{PSII}^{447} alone as a predictor of net PP in linear modelling approaches (Figure 5B).

497   Therefore, it is crucial that models consider the non-linear co-variation between net PP and σ_{PSII}^{447}

498   together with Chl-a in order to accurately predict net PP in this study area.

499   4.4 Modeling primary productivity by GAM

500   Modeling phytoplankton PP remains an important approach for oceanographers to better

501   understand marine ecosystem functioning. While several attempts including ours have been made

502   to estimate PP in the ECS, few works to date have focused on developing predictive models in the

503   Changjiang estuarine-coastal waters, due to the inadequate sampling resolution of incubation-

504   based approaches in such dynamic systems (Gong & Liu, 2003). Satellite-derived Chl-a has been

505   widely-used as an input into PP algorithms (Arrigo et al., 2011) yet there is not always a clear

506   relationship between phytoplankton biomass and production (Behrenfeld et al., 2005; Huot et al.,

507   2007; Laws et al., 2016). Efforts to estimate PP through scaling FRR-derived ETRs have gained

508   significant traction in recent years, however, are constrained by a still-limited understanding of

509   how K_C varies in nature (Lawrenz et al., 2013; Hughes et al. 2020). More recent work has

510   demonstrated the potential for fluorescence parameters relating to phytoplankton light history (e.g.,

511   NPQ) to correlate well with K_C (e.g., Schuback et al. 2015, 2016; Zhu et al., 2016; 2017); however,

512   the slope describing the relationship varies unpredictably in space and time (Hughes et al. 2018b)

513   or may break even down entirely under light-limited conditions (Hughes et al. 2021). Given the

514   inherent uncertainties in predicting K_C based off NPQ data, we opted to retrieve PP via a novel

515   modelling approach incorporating easy-to-measure fluorescence parameters and Chl-a. In the

516   current work, correlation analysis revealed that σ_{PSII} was negatively correlated with

517   photosynthetic rates in this highly-dynamic region. Thus, together with Chl-a which has been

518   routinely measured by fluorescence sensors (e.g. FRRf; Supplementary Figure S1), it provides an

519   opportunity to quickly assess variability of PP at high spatial resolution once the appropriate model

520   is established.

521   The empirical model of PP by stepwise multiple linear regression was first developed

522   including Chl-a and σ_{PSII}^{447}. The RMSE of SLR model was 248.7 mgC m^{-3} d^{-1}, which is close to that

523   of satellite-based empirical model developed in the ECS (Siswanto et al., 2006). Nevertheless,

524   negative values of PP were observed in the predicted results either due to particularly small Chl-a

525   or large σ_{PSII}^{447} values, highlight a notable drawback of linear models in such scenarios. In fact, the

526   growth rates of phytoplankton and the photosynthetic rates per unit Chl-a are not likely to infinitely

527   increase but at a decreasing rate when phytoplankton exhibit the so-called "package effect" (e.g.,

528   Laiolo et al. 2021) or photodamage conditions as well as insufficient nutrient supply (Cullen et al.,

529   1992; Platt et al., 1980; Siswanto et al., 2009), thus non-linear models are likely to better describe

530   C-fixation responses to changes in environmental variables (Siswanto et al., 2009). After fitting

531   data to a best GAM model, PP prediction was significantly improved through consideration of

532   non-linear relationships of Chl-a and σ_{PSII}^{447} on net PP, with RMSE decreasing from 248.7 to 144.2

533   mgC m^{-3} d^{-1} and R^2 increasing from 0.73 to 0.93, compared to the linear regression model (Tables

534   3, 4). This result confirms the robustness of the non-linear relationship between net PP and the two

535   fluorometric predictors. From initial setting with k-values of 3 on the σ_{PSII}^{447} and Chl-a smoothing,

536   we tested several combinations of k-values, showing the best-fitting GAM with k-values of 4 and

537   5 for σ_{PSII}^{447} and Chl-a, respectively. This suggests that the performance of GAM does not always

538   improve with increasing k-values, reinforcing recommendations by Wood (2018) to employ a

539   manual k-value selection process. It is also important to note that the selection of k-values is very

540   application-specific and should be re-evaluated with any new dataset (Murphy et al., 2019).

541   The developed PP model based on a GAM method in this study allows for assessment of

542   C-uptake rates at high spatial and temporal resolutions in the ECS – particularly with increasing

543   opportunities for ship-based sampling campaigns and use of autonomous measurement platforms

544   (Fujiki et al., 2008; Ryan-Keogh et al., 2020). The higher data volume afforded through our PP

545   model would not only benefit a better understanding of phytoplankton productivity in this dynamic

546   environment, but also be able to fill the large gaps in data required to validate satellite-based PP

547   models (Hughes et al., 2018a; Kerkar et al. 2021; Tripathy et al. 2012).

548

5 Conclusions

549 **5 Conclusions**

550   Our study found that surface PP in the Changjiang estuary and adjacent East China Sea

551   exhibits dramatic variability with a range spanning several orders of magnitude – highlighting the

552   dynamic nature of this system. According to our model, much of the variability in PP can be

553   predicted from knowledge of phytoplankton photophysiology and Chl-a biomass. Satellite models

554   routinely perform poorly in coastal systems, so development of high-resolution tools to assess PP

555   is an important step yielding greater understanding of carbon-cycling within this (and indeed other)

556   region(s). As active Chl-a fluorescence tools such as Fast Repetition Rate fluorometry become

557 smaller and less expensive, opportunities to deploy such instruments on vessels of opportunity,

558 gliders and other autonomous platforms are rapidly opening-up. If such sensors are calibrated to

559 measure *in-situ* chlorophyll-a concentration, our capacity to develop and utilize region-specific PP

560 estimation tools such as the one presented here can help fill the void of satellite-based PP models

561 which are so important in estimating phytoplankton productivity in other areas of the global ocean.

574 **Data Availability Statement**

575 Data set for this paper are freely available online through Figshare

576 (https://figshare.com/articles/dataset/Dataset_of_phytoplankton_primary_productivity_FRRf_Chl-

577 a_in_the_Changjiang_estuary_East_China_Sea/23691141).

578
579
580
581
582
583
584
585
586
587
588
589
590
591

Reference

Arrigo, K. R., DiTullio, G. R., Dunbar, R. B., Robinson, D. H., VanWoert, M., Worthen, D. L., & Lizotte, M. P. (2000), Phytoplankton taxonomic variability in nutrient utilization and primary production in the Ross Sea. *Journal of Geophysical Research: Oceans*, *105*(C4), 8827-8846.

Arrigo, K. R., van Dijken, G. L., and Bushinsky, S. (2008), Primary production in the Southern Ocean, 1997–2006. *Journal of Geophysical Research: Oceans*, *113*, C08004, doi:10.1029/2007JC004551.

Arrigo, K. R., & van Dijken, G. L. (2011), Secular trends in Arctic Ocean net primary production. *Journal of Geophysical Research: Oceans*, *116*(C9).

Behrenfeld, M. J. & Falkowski, P. G. (1997), Photosynthetic rates derived from satellite-based chlorophyll concentration. *Limnology and Oceanography*, *42*(1), 1–20.

Behrenfeld, M. J., Boss, E., Siegel, D. A., and Shea, D. M. (2005), Carbon-based ocean productivity and phytoplankton physiology from space. *Global Biogeochemical Cycles*, *19*, GB1006,doi:10.1029/2004gb002299.

Behrenfeld, M. J., Worthington, K., Sherrell, R. M., Chavez, F. P., Strutton, P., McPhaden, M., and Shea, D. M. (2006), Controls on tropical Pacific Ocean productivity revealed through nutrient stress diagnostics, *Nature*, *442*, 1025–1028.

Behrenfeld, M. J., O'Malley, R. T., Boss, E. S., Westberry, T. K., Graff, J. R., Halsey, K. H., et al. (2016), Revaluating ocean warming impacts on global phytoplankton. *Nature Climate Change*, *6*(3), 323–330. https://doi.org/10.1038/nclimate2838

Berges, J. A., Charlebois, D. O., Mauzerall, D. C., & Falkowski, P. G. (1996), Differential effects of nitrogen limitation on photosynthetic efficiency of photosystems I and II in microalgae. *Plant Physiology*, *110*(2), 689-696.

Browning, T. J., Bouman, H. A., Moore, C. M., Schlosser, C., Tarran, G. A., Woodward, E. M. S., et al. (2014), Nutrient regimes control phytoplankton ecophysiology in the South Atlantic. *Biogeosciences* 11, 463–479. doi: 10.5194/bg-11-463-2014

Cermeño, P, Estévez-Blanco P, Maranón E, Fernández. E. (2005), Maximum photosynthetic efficiency of size fractionated phytoplankton assessed by ^{14}C uptake and fast repetition rate fluorometry. *Limnology and Oceanography, 50*, 1438-1446.

Chang, J., Shiah, F.-K., Gong, G.-C., & Chiang, K. P. (2003), Cross-shelf variation in carbon-to-chlorophyll a ratios in the East China Sea, summer 1998. *Deep Sea Research Part II: Topical Studies in Oceanography, 50*, 1237-1247. https://doi.org/10.1016/S0967-0645(03)00020-1

Cheah, W., McMinn, A., Griffiths, F. B., Westwood, K. J., Wright, S. W. et al. (2011), Assessing Sub-Antarctic Zone primary productivity from fast repetition rate fluorometry. *Deep Sea Research Part II: Topical Studies in Oceanography*, *58*, 2179–2188.

Chen, Y.-L. L., Chen, H.-Y., Gong, G.-C., Lin, Y.-H., Jan, S., & Takahashi, M. (2004), Phytoplankton production during a summer coastal upwelling in the East China Sea. *Continental Shelf Research*, *24*, 1321-1338. https://doi.org/10.1016/j.csr.2004.04.002

Cloern, J. E., Foster, S. and Kleckner, A. (2014). Phytoplankton primary production in the world's estuarine-coastal ecosystems. *Biogeosciences*, *11*, 2477–2501. doi:10.5194/bg-11-2477-2014.

Cullen, J. J., Yang, X., & MacIntyre, H. L. (1992), Nutrient limitation of marine photosynthesis. *Primary productivity and biogeochemical cycles in the sea*, 69-88.

Cullen, J. J., and Davis, R. F. (2003), The blank can make a big difference in oceanographic measurements. *Limnology and Oceanography Bulletin, 12*, 29–35. doi: 10.1002/lob.200312229

Fasiolo, M., Nedellec, R., Goude, Y. and Wood, S.N. (2019), Scalable visualization methods for modern generalized additive models. *Journal of computational and Graphical Statistics*, 1-9.

Falkowski, P. G., Owens, T. G., Ley, A. C., & Mauzerall, D. C. (1981), Effects of growth irradiance levels on the ratio of reaction centers in two species of marine phytoplankton. *Plant Physiology*, *68*(4), 969-973.

Firme, G. F., Hughes, D. J., Laiolo, L., Roughan, M., Suthers, I. M. and Doblin, M. A. (2023), Contrasting phytoplankton composition and primary productivity in multiple mesoscale eddies along the East Australian coast. *Deep Sea Research Part I: Oceanographic Research*, *193*, p.103952.

Fisher, N.L., Campbell, D.A., Hughes, D.J., Kuzhiumparambil, U., Halsey, K.H., Ralph, P.J. and Suggett, D.J. (2020), Divergence of photosynthetic strategies amongst marine diatoms. *PLoS One*, 15(12), p.e0244252.

643 Fujiki, T., Hosaka, T., Kimoto, H., Ishimaru, T., Saino, T. (2008), In situ observation of phytoplankton productivity
644   by an underwater profiling buoy system: use of fast repetition rate fluorometry. *Marine Ecology Progress Series*,
645   *353*, 81–88.
646 Geider, R. J. (1987), Light and temperature dependence of the carbon to chlorophyll a ratio in microalgae and
647   cyanobacteria: implications for physiology and growth of phytoplankton. *New Phytologist*, 1-34.
648 Geider, R. J., La Roche, J., Greene, R. M., & Olaizola, M. (1993), Response of the photosynthetic apparatus of
649   Phaeodactylum tricornutum (Bacillariophyceae) to nitrate, phosphate, or iron starvation 1. *Journal of phycology*,
650   *29*(6), 755-766.
651 Geider, R. J., MacIntyre, H. L. & Kana, T. M. (1998a), A dynamic regulatory model of phytoplanktonic acclimation
652   to light, nutrients and temperature. *Limnology and Oceanography*, *43*, 679–694.
653 Geider, R. J., MacIntyre, H. L., Graziano, L. M., & McKAY, R. M. L. (1998b), Responses of the photosynthetic
654   apparatus of Dunaliella tertiolecta (Chlorophyceae) to nitrogen and phosphorus limitation. *European Journal of*
655   *phycology*, *33*(4), 315-332.
656 Gong, G. C., Shiah, F. K., Liu, K. K., Wen, Y. H., & Liang, M. H. (2000), Spatial and temporal variation of
657   chlorophyll a, primary productivity and chemical hydrography in the southern East China Sea. *Continental Shelf*
658   *Research*, *20*(4-5), 411-436.
659 Gong, G. C. & Liu, G.-J. (2003), An empirical primary production model for the ECS. *Continental Shelf Research*,
660   23, 213–224.
661 Gong, G. C., J. Chang, K. P. Chiang, T. M. Hsiung, C. C. Hung, S. W. Duan, and L. A. Codispoti. (2006),
662   Reduction of primary production and changing of nutrient ratio in the East China Sea: Effect of the Three Gorges
663   Dam?, *Geophysical Research Letters*, *33*, L07610, doi:10.1029/2006GL025800.
664 Grasshoff, K., Kremling, K., and Manfred, E. (1999), *Methods of seawater analysis* (NewYork: Wiley-VCH), 600.
665 Greene, R. M., Geider, R. J., Kolber, Z., Falkowski, P. G. (1992), Iron induced changes in light harvesting and
666   photochemical energy conversion processes in eukaryotic marine-algae. *Plant physiology,* 100, 565–575.
667 Guo, X., Miyazawa, Y., & Yamagata, T. (2006), The Kuroshio onshore intrusion along the shelf break of the East
668   China Sea: The origin of the Tsushima Warm Current. *Journal of Physical Oceanography*, *36*, 2205-2231.
669   https://doi.org/10.1175/JPO2976.1
670 Gutiérrez-Rodríguez, A., Safi, K., Fernández, D., Forcén-Vázquez, A., Gourvil, P., Hoffmann, L., ... & Nodder, S.
671   D. (2020), Decoupling between phytoplankton growth and microzooplankton grazing enhances productivity in
672   Subantarctic waters on Campbell Plateau, southeast of New Zealand. *Journal of Geophysical Research: Oceans*,
673   *125*(2), e2019JC015550.
674 Hancke, K., Dalsgaard, T., Sejr, M. K., Markager, S., Glud, R. N. (2015), Phytoplankton productivity in an Arctic
675   fjord (West Greenland): estimating electron requirements for carbon fixation and oxygen production. *PloS One*,
676   10,e0133275.
677 Hama, T., Miyazaki, T., Ogawa, Y., Iwakuma, T., Takahashi, M., Otsuki, A., Ichimura, S. (1983), Measurement of
678   photosynthetic production of a marine phytoplankton population using a stable ^{13}C isotope. *Marine Biology, 73*,
679   31-36.
680 Harding, L.W., Gallegos, C.L., Perry, E.S., Miller, W.D., Adolf, J.E., Mallonee, M.E., Paerl, H.W. (2016), Long-
681   term trends of nutrients and phytoplankton in Chesapeake bay. *Estuaries and Coasts*, *39* (3), 664–681.
682   https://doi.org/10.1007/s12237-015-0023-7.
683 Harding, L. W., Mallonee, M. E., Perry, E. S., David Miller, W., Adolf, J. E., Gallegos, C. L., & Paerl, H. W.
684   (2020), Seasonal to inter-annual variability of primary production in Chesapeake Bay: prospects to reverse
685   eutrophication and change trophic classification. *Scientific Reports*, *10*(1), 1-20.
686 Huang, R. X., and Russell, S. (1994), Ventilation of the subtropical North Pacific. *Journal of Physical*
687   *Oceanography*. 24, 2589–2605. doi: 10.1126/sciadv.abd1654
688 Hughes, D. J., Campbell, D., Doblin, M. A., Kromkamp, J., Lawrenz, E., Moore, C.M., et al. (2018a), Roadmaps and
689   Detours: Active chlorophyll-a assessments of primary productivity across marine and freshwater systems.
690   *Environmental Science & Technology, 52*, 12039–12054. doi: 10.1021/acs.est.8b03488
691 Hughes, D. J., Varkey, D., Doblin, M. A., Ingleton, T., Mcinnes, A., Ralph, P. J., et al. (2018b), Impact of nitrogen
692   availability upon the electron requirement for carbon fixation in Australian coastal phytoplankton communities.
693   *Limnology and Oceanography*, *63*, 1891–1910. doi: 10.1002/lno.10814
694 Hughes, D. J., Crosswell, J. R., Doblin, M. A., Oxborough, K., Ralph, P. J., Varkey, D., et al. (2020), Dynamic
695   variability of the phytoplankton electron requirement for carbon fixation in eastern Australian waters. *Journal of*
696   *Marine Systems, 202*, 103252. doi:10.1016/j.jmarsys.2019.103252

Hughes, D. J., Giannini, F. C., Ciotti, A. M., Doblin, M. A., Ralph, P. J., Varkey, D., et al. (2021). Taxonomic variability in the electron requirement for carbon fixation across marine phytoplankton. *Journal of Phycology. 57,* 111–127. doi: 10.1111/jpy.13068

Huner, N. P., Öquist, G., & Sarhan, F. (1998), Energy balance and acclimation to light and cold. *Trends in plant science*, *3*(6), 224-230.

Huot, Y., Babin, M., Bruyant, F., Grob, C., Twardowski, M. S., & Claustre, H. (2007), Does chlorophyll a provide the best index of phytoplankton biomass for primary productivity studies? *Biogeosciences discussions*, *4*(2), 707-745**.**

Jiang, Z., Liu, J., Chen, J., Chen, Q., Yan, X., Xuan, J., & Zeng, J. (2014), Responses of summer phytoplankton community to drastic environmental changes in the Changjiang (Yangtze River) estuary during the past 50 years. *Water Research*, *54*, 1-11. https://doi.org/10.1016/j.watres.2014.01.032

Jiang, Z., Chen, J., Zhou, F., Shou, L., Chen, Q., Tao, B., Yan, X., & Wang, K. (2015), Controlling factors of summer phytoplankton community in the Changjiang (Yangtze River) Estuary and adjacent East China Sea shelf. *Continental Shelf Research*, *101*, 71-84. https://doi.org/10.1016/j.csr.2015.04.009

Kameda, T., & Ishizaka, J. (2005), Size-fractionated primary production estimated by a two-phytoplankton community model applicable to ocean color remote sensing. *Journal of Oceanography*, 61, 663-672.

Kerkar, A.U., Tripathy, S.C., Hughes, D.J., Sabu, P., Pandi, S.R., Sarkar, A. and Tiwari, M. (2021), Characterization of phytoplankton productivity and bio-optical variability in a polar marine ecosystem. *Progress in Oceanography, 195, p.102573.*

Kolber, Z. S., Zehr, J., & Falkowski, P. (1988), Effects of growth irradiance and nitrogen limitation on photosynthetic energy conversion in photosystem II. *Plant physiology*, *88*(3), 923-929.

Kolber, Z. S, Falkowski, P. G, (1993), Use of active fluorescence to estimate phytoplankton photosynthesis in situ. *Limnology and Oceanography, 38*,1646–1665.

Kolber, Z. S., Prášil, O., and Falkowski, P. G. (1998), Measurements of variable chlorophyll fluorescence using fast repetition rate techniques: defining methodology and experimental protocols. *Biochimica et Biophysica Acta. 1367*, 88–106. doi: 10.1016/S0005-2728(98)00135-2

Kromkamp, J. C., Dijkman, N. A., Peene, J., Simis, S. G., Gons, H. J. (2008), Estimating phytoplankton primary production in Lake Ijsselmeer (The Netherlands) using variable fluorescence (PAM-FRRF) and C-uptake techniques. *European Journal of Phycology, 43*, 327–344.

Kruskopf, M. and Flynn, K. J. (2006), Chlorophyll content and fluorescence responses cannot be used to gauge reliably phytoplankton biomass, nutrient status or growth rate, *New Phytologist*, 169, 525–536.

Kulk, G., van de Poll, W. H., and Buma, A. G. (2018), Photophysiology of nitrate limited phytoplankton communities in Kongsfjorden, Spitsbergen. *Limnology and Oceanography, 63*, 2606–2617. doi: 10.1002/lno.10963

Laiolo, L., Matear, R., Soja-Woźniak, M., Suggett, D.J., Hughes, D.J., Baird, M.E. and Doblin, M.A., 2021. Modelling the impact of phytoplankton cell size and abundance on inherent optical properties (IOPs) and a remotely sensed chlorophyll-a product. *Journal of Marine Systems*, *213*, p.103460.

Lawrenz, E., Silsbe, G., Capuzzo, E., Ylöstalo, P., Forster, R. M., Simis, S. G., et al. (2013), Predicting the electron requirement for carbon fixation in seas and oceans. *PLoS One,* 8, e58137. doi: 10.1371/journal.pone.0058137

Laws, E. A., & Bannister, T. T. (1980), Nutrient-limited and light-limited growth of *Thalassiosira fluviatilis* in continuous culture, with implications for phytoplankton growth in the ocean. *Limnology and Oceanography*, 25(3), 457–473. https://doi.org/10.4319/lo.1980.25.3.0457

Laws, E. A., Bidigare, R. R., & Karl, D. M. (2016), Enigmatic relationship between chlorophyll a concentrations and photosynthetic rates at Station ALOHA. *Heliyon*, *2*(9), e00156. https://doi.org/10.1016/j.heliyon.2016.e00156

Lee, Z., Marra, J., Perry, M. J., & Kahru, M. (2015), Estimating oceanic primary productivity from ocean color remote sensing: A strategic assessment. *Journal of Marine Systems, 149*, 50-59. https://doi.org/10.1016/j.jmarsys.2014.11.015

Li, W., Ge, J., Ding, P., Ma, J., Glibert, P. M., & Liu, D. (2021), Effects of dual fronts on the spatial pattern of chlorophyll-a concentrations in and off the Changjiang River Estuary. *Estuaries and Coasts*, *44*, 1408-1418.

Liu, H., Xie, Y., Browning, T. J., Xu, F., & Huang, B. (2022), Phytoplankton photophysiology across tropical eddies: Deconvolving nutrient, light, and community signals. *Frontiers in Marine Science*, *9*.

Liu, X., Xiao, W., Landry, M. R., Chiang, K. P., Wang, L., & Huang, B. (2016), Responses of phytoplankton communities to environmental variability in the East China Sea. *Ecosystems*, *19*, 832-849.

751 Liu, X., Laws, E. A., Xie, Y., Wang, L., Lin, L., & Huang, B. (2019), Uncoupling of seasonal variations between
752 phytoplankton chlorophyll a and production in the East China Sea. *Journal of Geophysical Research:*
753 *Biogeosciences*, *124*, 2400–2415. https://doi.org/10.1029/2018JG004924
754 MacIntyre, J. G., Cullen, J. J., and Cembella, A. D. (1997), Vertical migration, nutrition and toxicity in the
755 dinoflagellate Alexandrium tamarense, *Marine Ecology Progress Series*, 148, 201–216.
756 Marañón, E., Behrenfeld, M. J., González, N., Mouriño, B., & Zubkov, M. V. (2003), High variability of primary
757 production in oligotrophic waters of the Atlantic Ocean: uncoupling from phytoplankton biomass and size
758 structure. *Marine Ecology Progress Series*, *257*, 1-11.
759 Marra, J. F. (2015), Ocean productivity: a personal perspective since the first Liege Colloquium. *Journal of Marine*
760 *Systems*, *147*, 3–8.
761 McKew, B. A., Davey, P., Finch, S. J., Hopkins, J., Lefebvre, S. C., Metodiev, M. V., et al. (2013), The trade-off
762 between the light-harvesting and photoprotective functions of fucoxanthin-chlorophyll proteins dominates light
763 acclimation in Emiliania huxleyi (clone CCMP 1516). *New Phytologist,* 200, 74–85. doi: 10.1111/nph.12373
764 Moore, C. M., Suggett, D., Holligan, P. M., Sharples, J., Abraham, E. R., Lucas, M. I., ... & Hydes, D. J. (2003),
765 Physical controls on phytoplankton physiology and production at a shelf sea front: a fast repetition-rate
766 fluorometer based field study. *Marine Ecology Progress Series*, *259*, 29-45.
767 Moore, C. M., Lucas, M. I., Sanders, R., and Davidson, R. (2005). Basin-scale variability of phytoplankton bio-
768 optical characteristics in relation to bloom state and community structure in the Northeast Atlantic. *Deep Sea*
769 *Research Part I: Oceanographic Research*, *52*, 401–419. doi: 10.1016/j.dsr.2004.09.003
770 Moore, C. M., Suggett, D. J., Hickman, A. E., Kim, Y-N., Tweddle, J. F. et al. (2006), Phytoplankton
771 photoacclimation and photoadaptation in response to environmental gradients in a shelf sea. *Limnology and*
772 *Oceanography*, *51*, 936–949.
773 Moore, C. M., Mills, M. M., Langlois, R., Milne, A., Achterberg, E. P. et al. (2008), Relative influence of nitrogen
774 and phosphorous availability on phytoplankton physiology and productivity in the oligotrophic sub-tropical North
775 Atlantic Ocean. *Limnology and Oceanography, 53*, 291–305.
776 Moreno-Madriñán, M. J., & Fischer, A. M. (2013), Performance of the MODIS FLH algorithm in estuarine waters: a
777 multi-year (2003–2010) analysis from Tampa Bay, Florida (USA). *International journal of remote sensing*,
778 *34*(19), 6467-6483.
779 Morelle, J., Schapira, M., Orvain, F., Riou, P., Lopez, P. J., Pierre-Duplessix, O., ... & Claquin, P. (2018), Annual
780 phytoplankton primary production estimation in a temperate estuary by coupling PAM and carbon incorporation
781 methods. *Estuaries and Coasts*, *41*, 1337-1355.
782 Murphy, R. R., Perry, E., Harcum, J., & Keisman, J. (2019), A generalized additive model approach to evaluating
783 water quality: Chesapeake Bay case study. *Environmental modelling & software*, *118*, 1-13.
784 Nielsen, E. S. (1952), The use of radio-active carbon (^{14}C) for measuring organic production in the sea. *Journal du*
785 *Conseil / Conseil Permanent International pour l'Exploration de la Mer*.*18*, 117–140. doi:
786 10.1093/icesjms/18.2.117
787 Ning, X., Vaulot, D., Zhensheng, L., & Zilin, L. (1988), Standing stock and production of phytoplankton in the
788 estuary of the Changjiang (Yangtse River) and the adjacent East China Sea. *Marine Ecology Progress Series*,
789 141-150. https://doi:10.3354/meps049141.
790 Ning, X., Liu, Z., Cai, Y., Fang, M., Chai, F. (1998), Physicobiological oceanographic remote sensing of the East
791 China Sea: satellite and in situ observations. *Journal of Geophysical Research: Oceans*, *103*, 21623–21635.
792 Osmond, C.B., 1994, What is photoinhibition? some insights from comparisons of shade and sun plants. In: Baker,
793 N.R., Bowyer, J.R. (Eds.), Photoinhibition of Photosynthesis from Molecular Mechanisms to the Field. *BIOS*
794 *Scientific Publishers*, Oxford, pp. 1–24
795 Oxborough, K., Moore, C. M., Suggett, D. J., Lawson, T., Chan, H. G. et al (2012), Direct estimation of functional
796 PSII reaction center concentration and PSII electron flux on a volume basis: a new approach to the analysis of
797 Fast Repetition Rate fluorometry (FRRf) data. *Limnology and Oceanography*: Methods, 10, 142–154.
798 Parkhill, J. P., Maillet, G., & Cullen, J. J. (2001), Fluorescence-based maximal quantum yield for PSII as a
799 diagnostic of nutrient stress. *Journal of Phycology*, *37*(4), 517-529.
800 Platt, T. & Jassby, A. D. (1976), The relationship between photosynthesis and light for natural assemblages of
801 coastal marine phytoplankton. *Journal of Phycology*, *12*, 421-430.
802 Platt, T., Gallegos, C. L., Harrison, W. G.(1980), Photoinhibition of photosynthesis in natural assemblages of marine
803 phytoplankton. *Journal of Marine Research*, *38*, 687–701.
804 R Core Team (2019), *R:* A Language and Environment for Statistical Computing. Vienna: R Foundation for
805 Statistical Computing.

806 Raateoja, M., Seppälä, J., Kuosa, H. (2004), Bio-optical modelling of primary production in the SW Finnish coastal
807   zone, Baltic Sea: fast repetition rate fluorometry in Case 2 waters. *Marine Ecology Progress Series*, *267*, 9–26.
808 Richards, R., Hughes, L., Gee, D., Tomlinson, R., (2013). Using generalized additive models for water quality
809   assessments: a case study example from Australia. *Journal of Coastal Research*, *111*, 116.
810   https://doi.org/10.2112/SI65-020.1.
811 Robinson, C., Suggett, D., Cherukuru, N., Ralph, P., Doblin, M. (2014), Performance of fast repetition rate
812   fluorometry based estimates of primary productivity in coastal waters. *Journal of Marine Systems, 139*, 299–310.
813 Ryan-Keogh, T. J., & Thomalla, S. J. (2020), Deriving a proxy for iron limitation from chlorophyll fluorescence on
814   buoyancy gliders. *Frontiers in Marine Science*, *7*, 275.
815 Schlitzer, R. (2018), Ocean Data View. Available online at: http://odv.awi.de
816 Schrader, P. S., Milligan, A. J., and Behrenfeld, M. J. (2011), Surplus Photosynthetic Antennae Complexes Underlie
817   Diagnostics of Iron Limitation in a Cyanobacterium, *Plos One*, 6, e18753, doi:10.1371/journal.pone.0018753.
818 Schuback, N., Schallenberg, C., Duckham, C., Maldonado, M. T., Tortell, P. D. (2015), Interacting effects of light and
819   iron availability on the coupling of photosynthetic electron transport and CO_2-assimilation in marine phytoplankton.
820   *PLoS One, 10*(7), e0133235.doi:10.1371/journal.pone.0133235.
821 Schuback, N., Flecken, M., Maldonado, M. T., & Tortell, P. D. (2016), Diurnal variation in the coupling of
822   photosynthetic electron transport and carbon fixation in iron-limited phytoplankton in the NE subarctic Pacific.
823   *Biogeosciences*, *13*,1019-1035.
824 Schuback, N., Hoppe, C. J, Tremblay, J. É, Maldonado, M. T., Tortell, P. D. (2017), Primary productivity and the
825   coupling of photosynthetic electron transport and carbon fixation in the Arctic Ocean. *Limnology and
826   Oceanography*, *62*,898-921.
827 Schuback, N., Tortell, P.D., Berman-Frank, I., Campbell, D.A., Ciotti, A., Courtecuisse, E., Erickson, Z.K., Fujiki,
828   T., Halsey, K., Hickman, A.E. and Huot, Y. (2021), Single-turnover variable chlorophyll fluorescence as a tool
829   for assessing phytoplankton photosynthesis and primary productivity: opportunities, caveats and
830   recommendations. *Frontiers in Marine Science*, *8*, p.690607.
831 Siswanto, E., Ishizaka, J., & Yokouchi, K. (2006), Optimal primary production model and parameterization in the
832   eastern East China Sea. *Journal of Oceanography*, *62*, 361-372.
833 Siswanto, E., Morimoto, A., & Kojima, S. (2009), Enhancement of phytoplankton primary productivity in the
834   southern East China Sea following episodic typhoon passage. *Geophysical Research Letters*, *36*(11).
835 Six, C., Finkel, Z., Rodriguez, F., Marie, D., Partensky, F., Campbell, D. A. (2008), Contrasting photoacclimatation
836   costs in ecotypes of the marine picoplankter Ostreococcus. *Limnology and Oceanography, 53*, 255–265.
837 Suggett, D. J., Maberly, S. C., and Geider, R. J. (2006), Gross photosynthesis and lake community metabolism
838   during the spring phytoplankton bloom. *Limnology and Oceanography, 51*, 2064–2076. doi:
839   10.4319/lo.2006.51.5.2064
840 Suggett, D. J., MacIntyrem H. L., Kanam T. M., Geider, R. J. (2009a), Comparing electron transport with gas
841   exchange: parameterising exchange rates between alternative photosynthetic currencies for eukaryotic
842   phytoplankton. *Aquatic Microbial Ecology, 56*, 147–162.
843 Suggett, D. J., Moore, C. M., Hickman, A. E., Geider, R. J. (2009b). Interpretation of fast repetition rate (FRR)
844   fluorescence: signatures of phytoplankton community structure versus physiological state. *Marine Ecology
845   Progress Series*, *376*, 1–19.
846 Suggett, D. J., Moore, C. M., Geider, R. J. (2011), Estimating aquatic productivity from active fluorescence
847   measurements. In: *Chlorophyll a fluorescence in aquatic sciences: methods and applications*, Chapter 6. Springer,
848   pp 103–115.
849 Smyth, T., Pemberton, K., Aiken, J., Geider, R. (2004), A methodology to determine primary production and
850   phytoplankton photosynthetic parameters from fast repetition rate fluorometry. *Journal* of *Plankton Research, 26*,
851   1337–1350
852 Testa, J. M., Murphy, R. R., Brady, D. C. and Kemp, W. M. (2018), Nutrient- and Climate-Induced Shifts in the
853   Phenology of Linked Biogeochemical Cycles in a Temperate Estuary. *Frontiers in Marine Science, 5*, 114.doi:
854   10.3389/fmars.2018.00114
855 Tripathy, S. C., Ishizaka, J., Siswanto, E., Shibata, T., Mino, Y. (2012), Modification of the vertically generalized
856   production model for the turbid waters of Ariake Bay, southwestern Japan. *Estuarine*, *Coastal and Shelf Science*,
857   *97*,66–77.
858 Waga, H., Fujiwara, A., Hirawake, T., Suzuki, K., Yoshida, K., Abe, H., & Nomura, D. (2022), Primary
859   productivity and phytoplankton community structure in surface waters of the western subarctic Pacific and the
860   Bering Sea during summer with reference to bloom stages. *Progress in Oceanography*, *201*, 102738.

861 Wei, Y., Zhao, X., Sun, J. and Liu, H. (2019), Fast Repetition Rate Fluorometry (FRRF) Derived Phytoplankton
862   Primary Productivity in the Bay of Bengal. *Frontiers in* Microbiology, 10, 1164. doi: 10.3389/fmicb.2019.01164
863 Welschmeyer, N. A. (1994), Fluorometric analysis of chlorophyll a in the presence of chlorophyll b and
864   pheopigments. *Limnology and Oceanography*, *39*(8), 1985-1992.
865 Wood, S. (2018), *Mgcv*, vol. 1. pp. 8–23. https://CRAN.R-project.org/package=mgcv.
866 Wong, G., Gong, G., Liu, K., & Pai, S. (1998), 'Excess nitrate' in the East China Sea. *Estuarine, Coastal and Shelf*
867   *Science*, 46, 411-418. https://doi.org/10.1006/ecss.1997.0287
868 Yadav, S., & Shukla, S. (2016), Analysis of k-fold cross-validation over hold-out validation on colossal datasets for
869   quality classification. In *2016 IEEE 6th International conference on advanced computing (IACC)* (pp. 78-83).
870   IEEE.
871 Yang, S., Han, X., Zhang, C., Sun, B., Wang, X., Shi, X. (2014), Seasonal changes in phytoplankton biomass and
872   dominant species in the Changjiang River Estuary and adjacent seas: General trends based on field survey data
873   1959–2009. *Journal of Ocean University of China*, *13*, 926–934.
874 Yoshikawa, T., & Furuya, K. (2008), Phytoplankton photosynthetic parameters and primary production in Japan Sea
875   and the East China Sea: Toward improving primary production models. *Continental Shelf Research*, *28*(7), 962-
876   976.
877 Zhu, Y., Ishizaka, J., Tripathy, S. C., Wang, S., Mino, Y., Matsuno, T., et al. (2016), Variation of the photosynthetic
878   electron transfer rate and electron requirement for daily net carbon fixation in Ariake Bay, Japan. *Journal of*
879   *Oceanography*, 72,761–777 doi: 10.1007/s10872-016-0370-4
880 Zhu, Y., Ishizaka, J., Tripathy, S. C., Wang, S., Sukigara, C., Goes, J., et al. (2017), Relationship between light,
881   community composition and the electron requirement for carbon fixation in natural phytoplankton. *Marine*
882   *Ecology Progress Series*, *580*, 83–100 doi: 10.3354/meps12310
883 Zhu, Y, Suggett, D. J, Liu, C., He, J., Lin, L., Le, F., Ishizaka, J., Goes, J. and Hao, Q. (2019), Primary Productivity
884   Dynamics in the Summer Arctic Ocean Confirms Broad Regulation of the Electron Requirement for Carbon
885   Fixation by Light-Phytoplankton Community Interaction. *Frontiers in Marine Science*. *6*, 275.doi:
886   10.3389/fmars.2019.00275.
887 Zhu, Y., Feng, Y., Browning, T. J., Wen, Z., Hughes, D. J., Ha,o Q., Zhang, R., Meng Q, Wells, M. L., Jiang, Z.,
888   Dissanayake, PAKN, Priyadarshani, W. N. C., Shou, L., Zeng, J. and Chai, F. (2022). Exploring Variability of
889   Trichodesmium Photophysiology Using Multi-Excitation Wavelength Fast Repetition Rate Fluorometry.
890   *Frontiers in Microbiology*, *13*, 813573.doi: 10.3389/fmicb.2022.81357
891 Zhu, Z. Y., Ng, W. M., Liu, S. M., Zhang, J., Chen, J. C., & Wu, Y. (2009), Estuarine phytoplankton dynamics and
892   shift of limiting factors: A study in the Changjiang (Yangtze River) Estuary and adjacent area. *Estuarine, Coastal*
893   *and Shelf Science*, *84*(3), 393-401.
894